Japanese Journal of Applied Physics

The Japan Society of Applied Physics

REGULAR PAPER

Local two-dimensional distribution of propagation speed of myocardial contraction for ultrasonic visualization of contraction propagation

Japanese Journal of Applied Physics **58**, SGGE05 (2019) **REGULAR PAPER**
https://doi.org/**10.7567/1347-4065/ab0d0b**

Local two-dimensional distribution of propagation speed of myocardial contraction for ultrasonic visualization of contraction propagation

Akane Hayashi[1], Shohei Mori[2], Mototaka Arakawa[1,2*], and Hiroshi Kanai[2,1]

[1]*Graduate School of Biomedical Engineering, Tohoku University, Sendai 980-8579, Japan*
[2]*Graduate School of Engineering, Tohoku University, Sendai 980-8579, Japan*

[*]E-mail: arakawa@ecei.tohoku.ac.jp

Received November 9, 2018; accepted January 15, 2019; published online June 11, 2019

The propagation of myocardial contraction caused by the conduction of electrical excitation in the heart has been visualized in our previous study. However, it was assumed that the contraction propagated parallel to the heart wall and the propagation speed was constant within the measurement area. In the present study, we estimated the two-dimensional propagation speed of contraction at each local area by ultrasonic measurement, and examined the mechanism of the contraction propagation in the heart by calculating the spatial distribution of the propagation speed vectors. By applying the proposed method to the interventricular septum of the human heart, the propagation speed in the lateral direction was approximately 1.6 times faster than that in the beam direction. The significant difference in propagation speeds between the specialized and ordinary myocardia was detected successfully. This study suggests that the proposed method can detect the myocardial ischemic and arrhythmia regions non-invasively. © 2019 The Japan Society of Applied Physics

1. Introduction

Approximately 9.4 million people worldwide die annually owing to heart diseases, and the number of deaths has been increasing.[1)] Heart disease ranks top in the cause of death and constitutes 17% of all-cause mortality. Therefore, the prevention of the onset of heart diseases and their appropriate treatments are essential, and the development of a diagnostic method that can be applied repeatedly with high accuracy is required urgently. Conventionally, chest X-ray,[2)] computed tomography,[3)] magnetic resonance imaging,[4,5)] and medical ultrasound are typically used for the diagnosis of heart diseases. Ultrasonic diagnosis using medical ultrasound is highly useful because it is non-invasive in vivo, the equipment is comparatively inexpensive, and the minute movements and temporal changes of organs and blood vessels can be captured repeatedly in real time.[6–13)]

The representative heart disease is an ischemic heart disease, and the important condition is myocardial infarction. The lesion where myocardial infarction occurs is known as the ischemic region, injured region, and infarct region in the order of disease progression.[14)] The ischemic region is the region where the coronary narrows and the blood does not reach the myocardium. Fatal necrosis of the myocardium can be avoided by prompt re-perfusion in the ischemic region. In the next stage, i.e., the injured region, it is barely possible to avoid myocardium necrosis. However, recovery cannot be expected in the infarct region in which the myocardium is necrotic when the coronary narrows further and becomes blocked. Therefore, the non-invasive and rapid identification of the myocardial ischemic region is crucial for the diagnosis and subsequent appropriate treatments in the early stages of ischemic heart diseases.

To detect and identify the myocardial ischemic regions, it is necessary to first clarify the characteristics of myocardium in the normal condition. Detection of the myocardial contraction response caused by the conduction of electrical excitation in the heart has been studied, and the excitation process and myocardium contraction caused by the excitation have been confirmed.[15–19)] We ultrasonically detected the pulsed minute vibration (displacement amplitude: 30 μm, velocity amplitude: 0.5 m s^{-1}) that occurred with the myocardial contraction at 15 ms after delivering an electrical stimulus in the papillary muscle extracted from an isolated rat heart.[20)] We measured the pulsed vibrations at about 10 000 points in the interventricular septum (IVS) in the time of conduction of the excitation at electrocardiographic QRS waves and at the occurrence of the first heart sound in the human heart, and confirmed the propagation of myocardial contraction.[21,22)] Moreover, we applied the ultrasonic measurement to both the IVS and left ventricular (LV) posterior wall in the human heart simultaneously, and confirmed the propagation of myocardial contraction along the conduction path of the electrical excitation.[23)]

Meanwhile, the detection and imaging of the myocardial ischemic regions have been studied.[24–29)] The propagation speed of the myocardial contraction response caused by the electrical excitation decelerated to 0.7 m s^{-1} in the ischemic region, whereas it was 1.2 m s^{-1} in the normal region in the open-chest canine heart.[30)] We applied our ultrasonic method to the IVS of open-chest swine hearts, and compared the propagation speeds of myocardial contraction in the normal and ischemic myocardia.[31,32)] The estimated propagation speeds were 2.7 m s^{-1} in the normal myocardium and 1.4 m s^{-1} in the ischemic myocardium, and we confirmed that the propagation speed of myocardial contraction decreased by approximately 50% owing to ischemia.

However, it was assumed that the myocardial contraction propagated parallel to the heart wall and the propagation speed was constant within the measurement range in our previous study. A more detailed visualization of the propagation of myocardial contraction is required to establish the diagnostic method for the detection of the myocardial ischemic regions and demonstrate the propagation of contraction occurring in the heart physiologically. Although the method of estimating the propagation speed vectors was proposed in the past,[33)] electrical activation of the myocardium was measured by electrodes attached to the epicardia in swine hearts, and the propagation of myocardial contraction was not measured non-invasively.

The propagation speed of myocardial contraction can be estimated by measuring the minute movements caused by

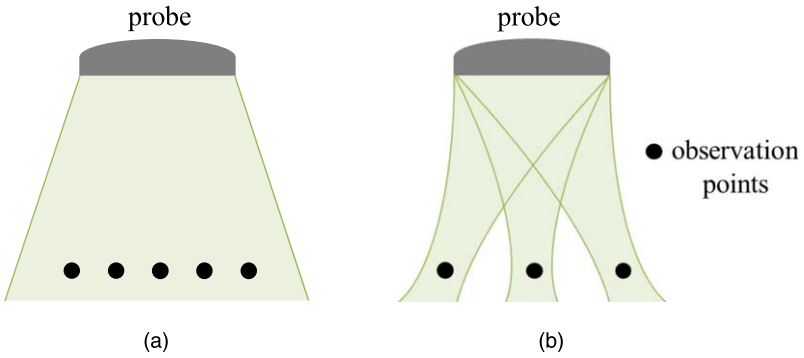

Fig. 1. (Color online) Transmission method of ultrasound. (a) Diverging wave and (b) focused wave.

contractions in the heart wall using ultrasound. The block matching method is used widely for measuring the movement.[34–36] In our previous study, the movement of the heart wall was measured by the block matching method, and the velocities with minute vibrations at multiple points in the myocardium were obtained.[37,38] This method enables movements to be tracked by applying the cross-correlation method to the speckle pattern within a region of interest (ROI) in successive frames. Therefore, it was necessary to measure the RF signals with high-frame rates and to acquire them densely in the lateral direction. The high-frame-rate measurement was realized by transmitting diverging or plane ultrasound waves, as shown in Fig. 1(a). The dense acquirement of the RF signals in the lateral direction was realized by forming the received beams densely. However, the amount of calculation increases in this method, and sophisticated diagnostic equipment is required. In addition, because the valves and the walls move quickly in the heart, the S/N decreases in the measurement using diverging or plane ultrasound waves. The measurement using focused waves is desirable to obtain the velocity with minute vibrations accurately at multiple points in the heart wall.

We realized the high-frame-rate measurement by transmitting focused waves sparsely, as shown in Fig. 1(b). The myocardial contraction response that is the movement of the IVS to the apical side and to the LV side, was confirmed at the onset of ventricular contraction.[39] In the present study, we measured the movement of the IVS to the LV side, i.e., the contraction response of the IVS in the beam direction on the LV long-axis view at several thousands of points, and confirmed that the measured contraction response propagated in the lateral and beam directions at each local area. Further, 25 ms were required for the myocardial contraction to propagate within the measurement range, assuming that the propagation speed of contraction was $4\,\mathrm{m\,s^{-1}}$, which is the upper limit of the conduction speed of electrical excitation,[40] and the measurement range of the propagation direction was 100 mm. The contraction propagation can be captured sufficiently by measuring using a frame rate of about 400 Hz. We estimated the two-dimensional propagation speed of myocardial contraction at each local area by ultrasonic measurement, and examined the mechanism of the contraction propagation in the heart by calculating the spatial distribution of the speed vectors. By increasing the number of subjects since the recent report,[41] we improved the reliability of the results, and discussed the results physiologically, in detail.

2. Methods

2.1. Measurement of velocity with minute vibrations in the myocardium

Because the focused waves were transmitted sparsely and the RF signals were not acquired densely in the lateral direction, the velocities with minute vibrations in the myocardium were obtained by applying the phased-tracking method.[42,43] The phase difference $\Delta\theta(t; l)$ of the received signals between the times t and $t + \Delta T$ at the center angular frequency ω_0 was calculated, and the velocity $v(t; l)$ with minute vibrations at each time t was obtained by

$$v(t; l) = \frac{c_0}{2\Delta T}\frac{\Delta\theta(t; l)}{\omega_0}, \tag{1}$$

where c_0 is the velocity of ultrasound in soft biological tissues, ΔT is the transmission interval of the ultrasonic pulse, and l is the distance from the center of surface of the ultrasound probe. The method stated above can be implemented with the current diagnostic equipment because only a small amount of calculation is involved.

Velocity waveforms with minute vibrations in the myocardium were obtained as shown in Fig. 2 by the phased-tracking method. Displacement waveforms obtained by integrating the velocity waveforms are also shown. Although several studies have reported the detection of myocardial contraction using displacement waveforms,[7,8,19,27,28,30,44–46] it is possible to measure not only the visible contraction but also minute vibrations caused by contraction using velocity waveforms. The contraction response at the time of the electrocardiographic QR interval representing the onset of ventricular contraction can be identified as the bimodal movements of myocardium toward the LV, i.e., the bimodal positive waveform in velocity waveforms, although the displacement waveforms were almost smooth. The bimodality of the contraction response has also been confirmed in our previous study,[31] and the event was associated with the myocardium contraction. It is possible to accurately detect the myocardial contraction response by analyzing the velocity waveforms with minute vibrations in the myocardium. Therefore, the velocity waveforms are useful for estimation of the two-dimensional propagation speed of myocardial contraction at each local area.

2.2. Delay time measurement of myocardial contraction response[23,32]

The velocity waveforms of the beam direction with minute vibrations were obtained simultaneously at several thousands of points in the myocardium by the phased-tracking

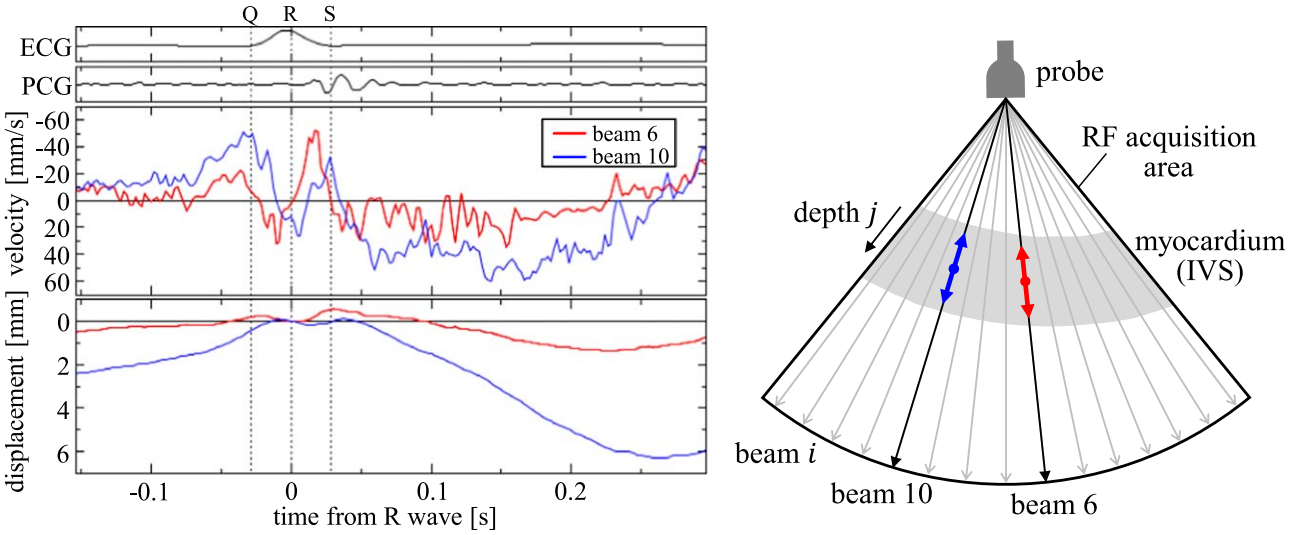

Fig. 2. (Color online) Electrocardiogram (ECG), phonocardiogram (PCG), velocity waveforms with minute vibrations and displacement waveforms in interventricular septum.

method.[42,43] The arrival time difference of the contraction response was calculated using the velocity waveforms $v(t; l_0)$ with minute vibrations at the reference position l_0 and $v(t; l_{ij})$ at the position l_{ij} with the beam i and depth j from the probe. The reference position l_0 was set at the measurement position where the amplitude of the velocity waveform was the maximum in the correlation window among all the measured velocity waveforms. The delay time τ_p of the contraction response $v(t; l_{ij})$ at each position l_{ij} from the contraction response $v(t; l_0)$ at the reference position l_0 was determined by applying the cross-correlation method. The calculated delay time τ_p from the reference waveform $v(t; l_0)$ was converted into the delay time τ_{ij} [s] from the electrocardiographic R wave representing the onset of ventricular contraction. The differences in the delay time of the contraction responses can be compared among multiple measurements by unifying the criteria for calculating the delay time.

In the electrocardiographic QR interval at the onset of ventricular contraction, the peak at which the myocardium moved to the LV, i.e., the velocity with minute vibrations became positive, was regarded as the contraction response, and the center of correlation window was set at that time. The width of the correlation window was set to be the same as the width of the contraction response waveform, and the search area, that is the range to move the correlation window was limited to approximately 25 ms before and after the correlation window. The propagation time of myocardial contraction within the measurement range was calculated as 25 ms assuming that the propagation speed of contraction was $4\,\mathrm{m\,s^{-1}}$, which is the upper limit of the conduction speed of electrical excitation,[40] and the measurement range of propagation direction was 100 mm.

2.3. Propagation speed estimation of myocardial contraction response

In Cartesian coordinates, the calculated delay time distribution $\{\tau_{ij}\}$ of the myocardial contraction response was expressed as (x, y, τ_{xy}) by the measurement position (x, y) and delay times $\{\tau_{xy}\}$. A quadratic surface $T(x, y)$ was fitted by the weighted least-squares method in the ROI centered at each measurement position (x_0, y_0), as shown in Fig. 3. The surface $T(x, y)$ was given by

$$T(x, y) = a + bx + cy + dx^2 + exy + fy^2, \tag{2}$$

where a, b, c, d, e, and f are coefficients. In the present study, the size of the ROI for fitting the quadratic surface $T(x, y)$ was 7.7 mm in the beam direction and five beams in the lateral direction. If the size of ROI is enlarged than the region that the quadratic surface can be fitted to the delay time distribution, the result becomes insufficient to fit the delay time distribution because of the lack of the degree in the fitting function, and the estimated result of $T(x, y)$ becomes averaged. The delay time distribution within a ROI is shown in Fig. 3, and it was judged that the quadratic surface can be appropriately fitted. The ROI along the delay time was not limited, and the correlation value for the reference waveform in the calculation of the delay time τ_p was used as the weight for fitting $T(x, y)$ in contrast to the resent report.[41] Then, the variability in the propagation speed vectors was further reduced.

The two-dimensional propagation speed of myocardial contraction was subsequently calculated using the gradient of the surface $T(x, y)$. The gradient vector was expressed as $\nabla T = [\partial T/\partial x,\ \partial T/\partial y]^T$, and the propagation speed $\boldsymbol{v}_e(x_0, y_0)$ was estimated by

$$\boldsymbol{v}_e(x_0, y_0) = \begin{bmatrix} \dfrac{dx}{dT} \\ \dfrac{dy}{dT} \end{bmatrix} = \begin{bmatrix} \dfrac{T_x}{T_x^2 + T_y^2} \\ \dfrac{T_y}{T_x^2 + T_y^2} \end{bmatrix}, \tag{3}$$

where $T_x = \partial T/\partial x$ and $T_y = \partial T/\partial y$.[33,46]

Because the local and two-dimensional propagation speed of myocardial contraction was estimated although only the average speeds were estimated in our previous study,[23,31,32] the estimation of spatial distribution of the propagation speed vectors became possible.

3. In vivo experiment

3.1. Experiment environment

In vivo measurement was applied to the IVS of three healthy males in their early 20 s using an ultrasound diagnostic

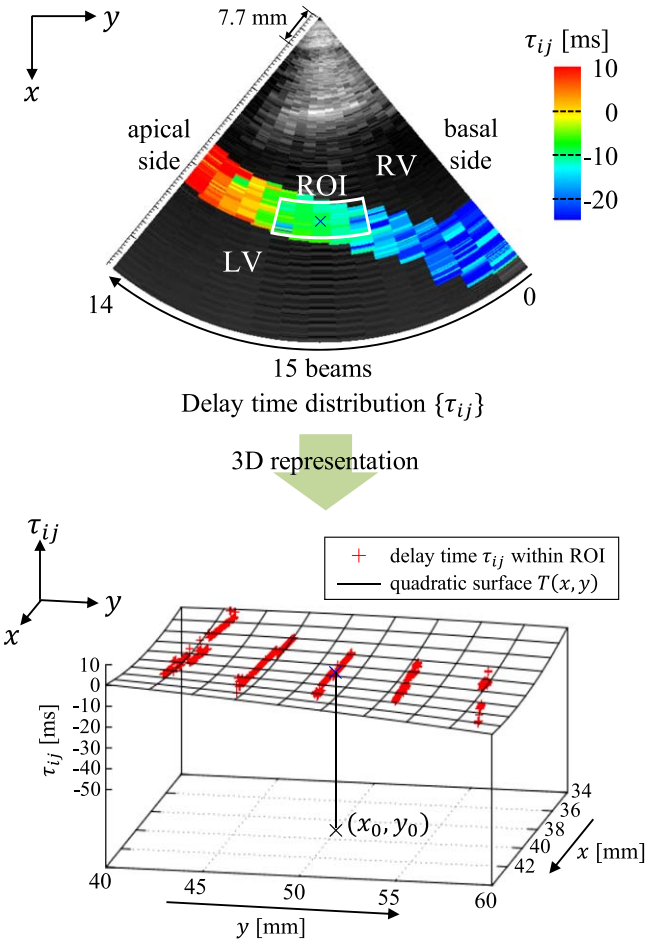

Fig. 3. (Color online) Quadratic surface fitting to delay time distribution $\{\tau_{ij}\}$.

equipment (SSD-6500, Aloka) with a sector probe of 5-MHz center frequency. The transmission pulse repetition frequency was 6510 Hz, and the high-frame-rate measurement of 434 Hz was realized by reducing the number of beams to 15. The sampling frequency was 20 MHz and the angle between successive beams was 5.6°. The measurement interval in the beam direction was 38.5 μm because the velocity c_0 of ultrasound in the soft biological tissue was assumed to be 1540 m s^{-1}. Figure 4 shows the acquired B mode image and the acquisition area of the RF data. The beam in the basal side in the heart was beam 0, and that in the apical side was beam 14. The B mode image in Fig. 4(a) was acquired with the frame rate of 63 Hz and 103 beams to identify the position of the IVS.

3.2. Results

Figure 5 shows the delay time distribution $\{\tau_{ij}\}$ of the myocardial contraction response. The reference position l_0 was set at approximately 33 mm in the depth from the probe in beam 7. The delay time increased from the basal side (beam 0) toward the apical side (beam 14), i.e., the myocardial contraction response propagated from the basal to apical sides, as in our previous study.[23)]

Figure 6 shows the estimated result of the propagation speed vectors $\{\boldsymbol{v}_e(x_0, y_0)\}$. The direction and magnitude of the propagation speeds were indicated by the direction and color of the arrows, respectively. The speed vector was indicated every 30 measurement positions in the beam direction. The propagation speed was represented as the speed vector in each ROI such that the local and two-dimensional estimation of the propagation speed became possible.

Figure 7 shows the result of decomposing the estimated propagation speed vector $\{\boldsymbol{v}_e(x_0, y_0)\}$ to the lateral and beam directions at each position. The propagation to the apical side (beam 14) was defined as positive in the lateral direction, and the propagation to the LV side was defined as positive in the beam direction. Focusing on the propagation in the lateral direction, the contraction propagated from the basal to apical sides in beams 3–14. Meanwhile, focusing on the propagation in the beam direction, the contraction propagated from the LV to right ventricle (RV) sides in beams 4–14. Moreover, the absolute values of the propagation speed were averaged in beams 4–14 where the contraction propagation was confirmed. They were approximately 1.1 m s^{-1} and 0.5 m s^{-1} in the lateral and beam directions, respectively. The propagation speed in the lateral direction was faster than that in the beam direction.

The data for other heartbeats of the same subject and multiple heartbeats of two other subjects were analyzed similarly. Similar results were obtained for the delay time distribution $\{\tau_{ij}\}$ and propagation speed vectors $\{\boldsymbol{v}_e(x_0, y_0)\}$. Figure 8 shows the propagation speed in the lateral and beam directions at each position in five heartbeats for three subjects. The propagation speed in the lateral direction was distinctively faster than that in the beam direction in all subjects. The average propagation speeds in the lateral and beam directions were 1.1 ± 0.3 m s^{-1} and 0.7 ± 0.3 m s^{-1}, respectively. The propagation speed in the lateral direction was approximately 1.6 times faster than that in the beam direction.

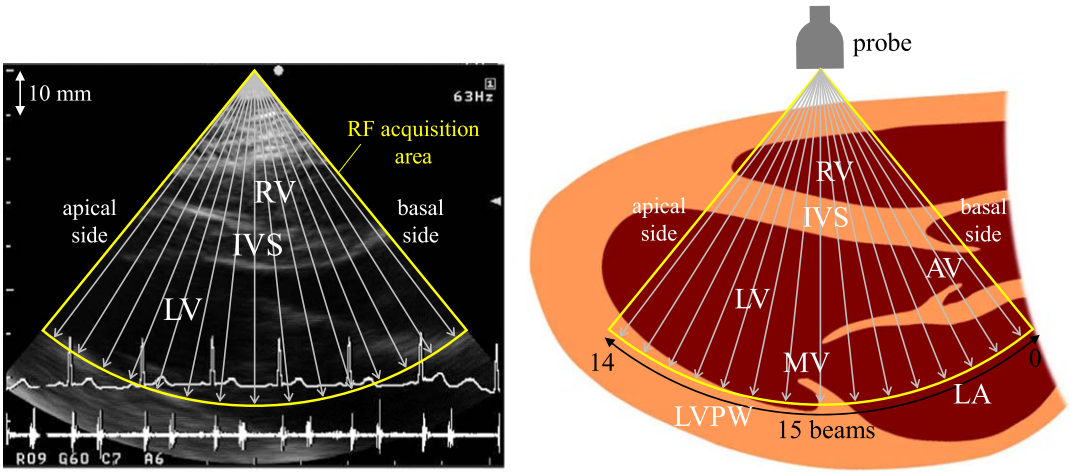

Fig. 4. (Color online) (a) B mode image[41] and (b) schematic diagram of measurement (IVS: interventricular septum, RV: right ventricle, LV: left ventricle, LVPW: left ventricular posterior wall, LA: left atrium, AV: aortic valve, MV: mitral valve).

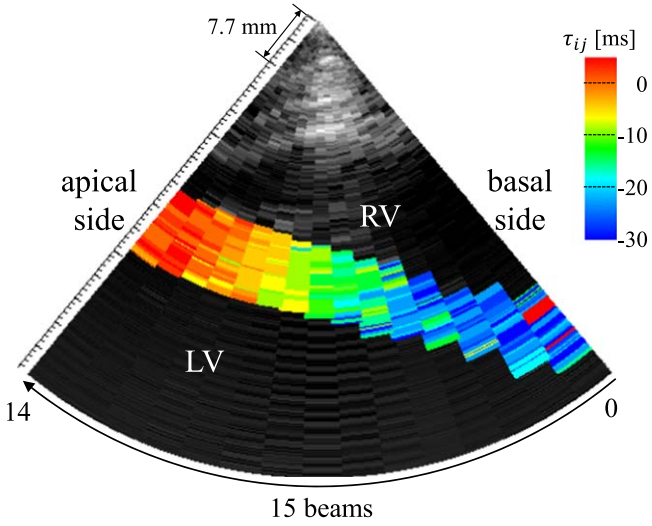

Fig. 5. (Color online) Delay time distribution $\{\tau_{ij}\}$ of myocardial contraction responses.

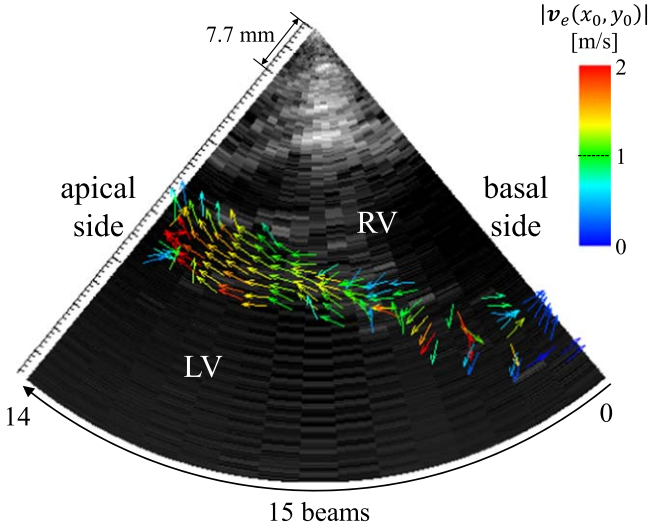

Fig. 6. (Color online) Propagation speed vectors $\{\boldsymbol{v}_e(x_0, y_0)\}$ of myocardial contraction.

4. Discussion

In the human heart, electrical excitation occurs in the sinoatrial node near the right atrium, and its excitation propagates through the specialized myocardium (conducting system) such as the atrioventricular node, bundle of His, bundle branch, and Purkinje fiber, as shown in Fig. 9. The surrounding ordinary myocardium which constitutes the walls in the atrium and the ventricle contracts by the electrical excitation in the specialized myocardium, and the heart acts as a pump to bring blood to all parts of the body. The propagation speeds of myocardial contraction in the bundle branch and Purkinje fiber inside the IVS were reported to be approximately 2–4 m s^{-1} from the basal to apical sides.[40] Meanwhile, that in the ordinary myocardium was reported to be approximately 0.3–1 m s^{-1}.[40,47]

In the lateral direction, the myocardial contraction propagated from the basal to apical sides in beams 3–14, as shown in Fig. 7(a). In beams 3–14, because the specialized myocardium runs inside the IVS laterally,[14,40,47] the propagation direction of contraction coincided with that of the electrical excitation that causes the myocardial contraction. Meanwhile, in the beam direction, the contraction propagated from the LV to RV sides in beams 4–14, as shown in Fig. 7(b). The right bundle branch (RBB) and left bundle branch (LBB) are the specialized myocardia in the RV and LV sides, respectively, on the surface of the IVS. Each bundle branch is connected to each Purkinje fiber. The RBB appears as a multifilament with 1–2 mm in diameter in the RV side on the surface of the IVS, whereas the LBB spreads like a fan widely in the LV side.[14,48,49] The RBB is difficult to be included in the ultrasonic measurement surface, whereas the LBB is easily included in it. When the RBB is not captured and only the LBB is captured by measurement, the propagation of contraction from the LBB is mainly measured, then the propagation from the LV to RV sides is observed. Therefore, it appears that the contraction propagation from the LBB and Purkinje fiber having a large distribution range was measured dominantly in the beam direction. Additionally, the presence of the specialized

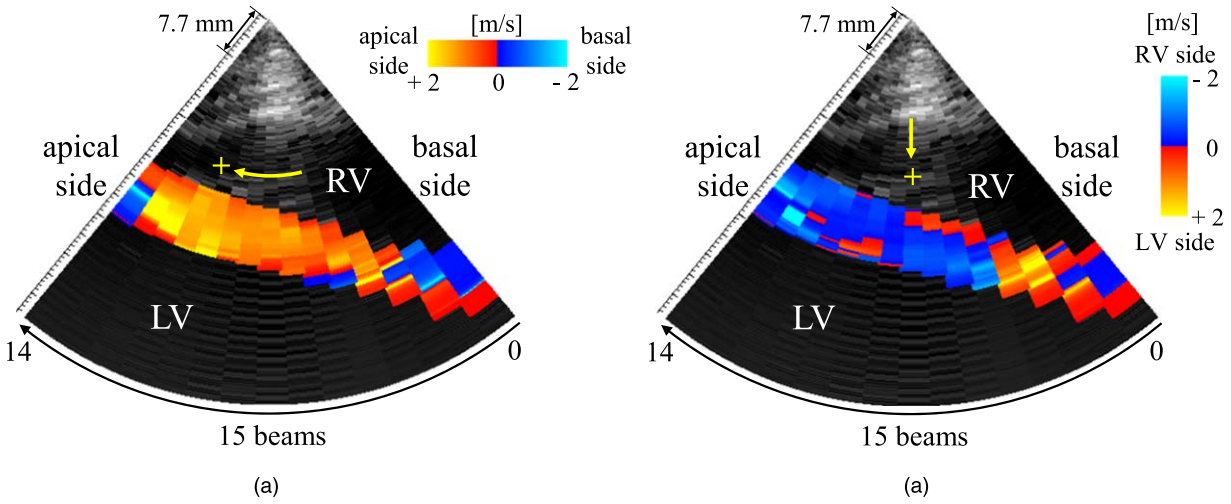

Fig. 7. (Color online) Propagation speeds of myocardial contraction in (a) lateral direction (positive: apical side) and (b) beam direction (positive: LV side).

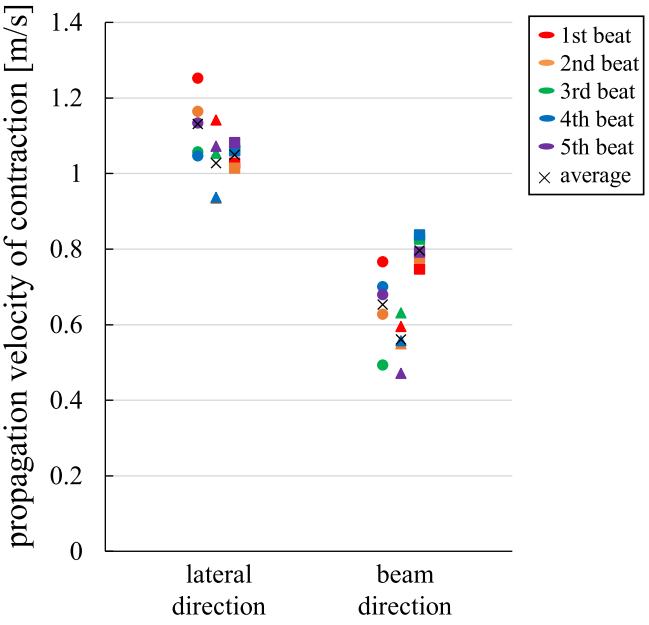

Fig. 8. (Color online) Average propagation speeds of myocardial contraction in (a) lateral direction and (b) beam direction in multiple heartbeats (●: subject A, ▲: subject B, ■: subject C).

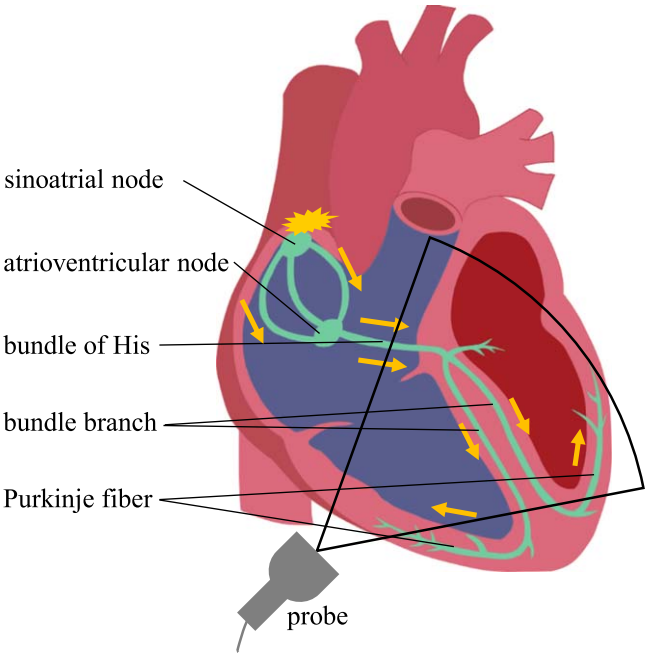

Fig. 9. (Color online) Schematic view of conduction of electrical excitation in human heart.

myocardium was indicated by the propagation speed in the lateral direction in beam 3. The propagation speed in the beam direction indicated the propagation from the RV to LV sides in beam 3 contrary to the propagation direction in beams 4–14. The vectors in the lower left direction can be similarly observed in beam 3 in Fig. 6. This is certainly because the position where the specialized myocardium entered into the IVS from the RV side was near beam 3, as shown in Fig. 9. Because the specialized myocardium entered into the IVS with lower left direction to the beam direction, the contraction propagation of the positive component was measured in the lateral and beam directions, respectively.

The estimated direction of propagation in the beam direction varied significantly than that in the lateral direction. This is certainly because the estimation range of propagation speed was approximately 20 mm, corresponding to five beams in the lateral direction and 7.7 mm corresponding to 200 measurement points in the beam direction, and the range was insufficient to estimate the propagation speed in the beam direction accurately. Because the IVS thickness is approximately 7–12 mm, it is difficult to further expand the estimation range in the beam direction. Further investigations would be required to estimate the propagation speed of contraction in the beam direction accurately.

Moreover, the propagation speeds in the lateral and beam directions were $1.1 \pm 0.3\ \mathrm{m\,s^{-1}}$ and $0.7 \pm 0.3\ \mathrm{m\,s^{-1}}$, respectively, and the propagation speed in the lateral direction was approximately 1.6 times faster than that in the beam direction. As mentioned above, the propagation speed of the specialized myocardium is reported to be faster than that of the ordinary myocardium.[40,47] The contraction propagation in the lateral direction was affected by the specialized myocardium that runs laterally, whereas the contraction propagation in the beam direction reflected that in the ordinary myocardium. Therefore, the result indicates that the propagation speed in the lateral direction is faster than that in the beam direction.

In the present study, the quadratic surface $T(x, y)$ was fitted to the delay time distribution within the ROI (7.7 mm × 5 beams) at each measurement position (x_0, y_0). However, the further investigation about the size of the ROI and the fitting function are still needed. The appropriate fitting conditions could be proposed by changing the conditions and evaluating variability in the results among multiple heartbeats of the same subject under each condition.

5. Conclusion

In the present study, we estimated the local and two-dimensional propagation speeds of myocardial contraction, and examined the mechanism of the contraction propagation in the heart by calculating the spatial distribution of the speed vectors. The spatial distribution of the propagation speed vectors of myocardial contraction was estimated, and the contraction propagation in the IVS was visualized in detail compared to the conventional method. Moreover, the propagation speeds in the lateral and beam directions were estimated as 1.1 and 0.7 m s^{-1}, respectively. The significant difference in propagation speeds between the specialized myocardium and ordinary myocardium were detected successfully.

The propagation of myocardial contraction reflected that of electrical excitation. Therefore, if the propagation of myocardial contraction could be visualized in detail by the proposed method, the identification of the myocardial ischemia region, and the detection of arrhythmia could be expected. In addition to the abnormality of the conducting system, the propagation of myocardial contraction when the abnormality occurred could also be visualized.

ORCID iDs

Shohei Mori https://orcid.org/0000-0002-5494-1055
Mototaka Arakawa https://orcid.org/0000-0001-9386-645X
Hiroshi Kanai https://orcid.org/0000-0002-6567-1687

1) Global Health Estimates, Deaths by Cause, Age, Sex, by Country and by Region, 2000-2016 World Health Organization, Geneva, 2018.
2) A. Battler, J. S. Karliner, C. B. Higgins, R. Slutsky, E. A. Gilpin, V. F. Froelicher, and J. Ross Jr., Circulation **61**, 1004 (1980).
3) L. T. Mahoney, W. Smith, M. P. Noel, M. Florentine, D. J. Skorton, and S. M. Collins, Invest. Radiol. **22**, 451 (1987).
4) L. Axel and L. Dougherty, Radiology **171**, 841 (1989).
5) M. B. Buchalter, J. L. Weiss, W. J. Rogers, E. A. Zerhouni, M. L. Weisfeldt, R. Beyar, and E. P. Shapiro, Circulation **81**, 1236 (1990).
6) G. R. Sutherland, G. D. Salvo, P. Claus, J. D'hooge, and B. Bijnens, J. Am. Soc. Echocardiogr. **17**, 788 (2004).
7) S. Wang, W. N. Lee, J. Provost, J. Luo, and E. E. Konofagou, IEEE Trans. Ultrason. Ferroelectr. Freq. Control **55**, 2221 (2008).
8) E. E. Konofagou, J. Luo, D. Saluja, D. O. Cervantes, J. Coromilas, and K. Fujikura, Ultrasonics **50**, 208 (2010).
9) Y. F. Cheung, Nat. Rev. Cardiol. **9**, 644 (2012).
10) K. Takahashi, H. Taki, and H. Kanai, Jpn. J. Appl. Phys. **56**, 07JF09 (2017).
11) M. Maeda, R. Nagaoka, H. Ikeda, S. Yaegashi, and Y. Saijo, Jpn. J. Appl. Phys. **57**, 07LF02 (2018).
12) K. Kaburaki, M. Mozumi, and H. Hasegawa, Jpn. J. Appl. Phys. **57**, 07LF03 (2018).
13) H. J. Vos, M. Strachinaru, B. M. van Dalen, I. Heinonen, J. Bercoff, J. G. Bosch, D. J. Duncker, A. F. W. van der Steen, and N. de Jong, IEEE Int. Ultrasonics Symp., 2016.
14) F. H. Netter, *The CIBA Collection of Medical Illustrations: Heart* (CIBA, Basel, 1975).
15) D. Durrer, R. T. Van Dam, G. E. Freud, M. J. Janse, F. L. Meijler, and R. C. Arzbaecher, Circulation **41**, 899 (1970).
16) J. C. Wood and D. T. Barry, Proc. IEEE **84**, 1281 (1996).
17) C. Ramanathan, R. N. Ghanem, P. Jia, K. Ryu, and Y. Rudy, Nat. Med. **10**, 422 (2004).
18) T. Arts, F. W. Prinzen, T. Delhaas, J. R. Milles, A. C. Rossi, and P. Clarysse, IEEE Trans. Med. Imaging **29**, 1114 (2010).
19) J. Grondin, E. Wan, A. Gambhir, H. Garan, and E. E. Konofagou, IEEE Trans. Ultrason. Ferroelectr. Freq. Control **62**, 337 (2015).
20) H. Kanai, S. Katsumata, H. Honda, and Y. Koiwa, Acoust. Sci. Technol. **24**, 17 (2003).
21) H. Kanai, IEEE Trans. Ultrason. Ferroelectr. Freq. Control **51**, 1931 (2005).
22) H. Kanai, Ultrasound Med. Biol. **35**, 936 (2009).
23) A. Hayashi, M. Arakawa, and H. Kanai, Jpn. J. Med. Ultrason. **45**, 191 (2018) [in Japanese].
24) O. J. Elle, S. Halvorsen, M. G. Gulbrandsen, L. Aurdal, A. Bakken, E. Samset, H. Dugstad, and E. Fosse, Physiol. Meas. **26**, 429 (2005).
25) Z. Yang, H. Zhang, S. Kong, X. Yue, Y. Jin, J. Jin, and Y. Huang, Physiol. Meas. **28**, 481 (2007).
26) C. Tronstad, S. E. Pischke, L. Holhjem, T. I. Tønnessen, Ø. G. Martinsen, and S. Grimnes, Physiol. Meas. **31**, 1241 (2010).
27) W. N. Lee, J. Provost, K. Fujikura, J. Wang, and E. E. Konofagou, Phys. Med. Biol. **56**, 1155 (2011).
28) J. Provost, V. T. Nquyen, D. Legrand, S. Okrasinski, A. Costet, A. Gambhir, H. Garan, and E. E. Konofagou, Phys. Med. Biol. **56**, L1 (2011).
29) D. Romero, J. P. Martinez, P. Laguna, and E. Pueyo, Physiol. Meas. **37**, 1004 (2016).
30) E. E. Konofagou, S. Fung-kee-Fung, J. Luo, and M. Pernot, Proc. 28th IEEE EMBS Annu. Int. Conf., 2006, p. 6648.
31) Y. Matsuno, H. Taki, H. Yamamoto, M. Hirano, S. Morosawa, H. Shimokawa, and H. Kanai, Jpn. J. Appl. Phys. **56**, 07JF05 (2017).
32) A. Hayashi, M. Arakawa, H. Yamamoto, S. Morosawa, H. Shimokawa, and H. Kanai, Jpn. J. Med. Ultrason. **45**, 595 (2018) [in Japanese].
33) P. V. Bayly, B. H. KenKnight, J. M. Rogers, R. E. Hillsley, R. E. Ideker, and W. M. Smith, IEEE Trans. Biomed. Eng. **45**, 563 (1998).
34) C. Zhu, X. Lin, and L. P. Chau, IEEE Trans. Circuits Syst. Video Technol. **12**, 349 (2002).
35) G. Zahnd, M. Orkisz, A. Serusclat, P. Moulin, and D. Vray, Med. Image Anal. **17**, 573 (2013).
36) T. Y. Lai, H. I. Chen, C. C. Shih, L. C. Kuo, H. Y. Hsu, and C. C. Huang, Med. Phys. **43**, 148 (2016).
37) Y. Honjo, H. Hasegawa, and H. Kanai, Jpn. J. Appl. Phys. **49**, 07HF14 (2010).
38) Y. Honjo, H. Hasegawa, and H. Kanai, Jpn. J. Appl. Phys. **51**, 07GF06 (2012).
39) I. Kobayashi, S. Mori, M. Arakawa, and H. Kanai, IEEE Int. Ultrasonics Symp., 2018.
40) D. M. Bers, *Excitation-Contraction Coupling and Cardiac Contractile Force* (Kluwer Academic, Boston, 2001), p. 64.
41) A. Hayashi, S. Mori, M. Arakawa, and H. Kanai, Proc. Symp. Ultrason. Electron. **39**, 3P5-1 (2018).
42) H. Kanai, M. Sato, Y. Koiwa, and N. Chubachi, IEEE Trans. Ultrason. Ferroelectr. Freq. Control **43**, 791 (1996).
43) H. Kanai, H. Hasegawa, N. Chubachi, Y. Koiwa, and M. Tanaka, IEEE Trans. Ultrason. Ferroelectr. Freq. Control **44**, 752 (1997).
44) Y. Seo, H. Yamasaki, R. Kawamura, T. Ishizu, M. Igarashi, Y. Sekiguchi, H. Tada, and K. Aonuma, Circulation J. **77**, 2481 (2013).
45) C. Papadacci, E. A. Bunting, E. Y. Wan, P. Nauleau, and E. E. Konofagou, IEEE Trans. Med. Imaging **36**, 618 (2017).
46) A. Costet, L. Melki, V. Sayseng, N. Hamid, K. Nakanishi, E. Wan, R. Hahn, S. Hamma, and E. E. Konofagou, Phys. Med. Biol. **62**, 9341 (2017).
47) F. W. Prinzen and M. Peschar, Pacing Clin. Electrophysiol. **25**, 484 (2002).
48) A. M. Katz, *Physiology of the Heart* (Lippincott Williams & Wilkins, Philadelphia, 2001) 3rd ed., p. 522.
49) H. Hayakawa and K. Hiejima, *Clinical Cardiac Electrophysiology* (Nankodo, Tokyo, 2001) 3rd ed., p. 18 [in Japanese].